Comparative Medicine
Copyright 2004
by the American Association for Laboratory Animal Science

Vol 54, No 4
August 2004
Pages 422-433

Subacute Necrotizing Encephalopathy in a Pig-tailed Macaque (*Macaca nemestrina*) That Resembles Mitochondrial Encephalopathy in Humans

Helle Bielefeldt-Ohmann, DVM, PhD,[1,*] Rita U. Bellanca,[1] Carolyn M. Crockett, PhD,[1] Eliza Curnow,[1] Kathy Eiffert,[1] Maggie Gillen, DVM,[1] Debra Glanister,[1] Eric Hayes, PhD,[1] Stephen Kelley, DVM,[1] Satoshi Minoshima, MD, PhD,[1,2] and Keith Vogel, DVM[1]

A male pig-tailed macaque (*Macaca nemestrina*), approximately 5 years old, was found to be vision-impaired and to have profound behavioral abnormalities, including hyperactivity and self-injurious behavior that was not amenable to amelioration by environmental enrichment. Facial and skeletal dysmorphisms also were noted. Magnetic resonance imaging (MRI) and positron emission tomography (PET) scanning revealed areas of possible infarction in the occipital lobes and megaventriculosis. At necropsy, following euthanasia for humane reasons, severe polio- and leukoencephalomalacia accompanied by megaventriculosis were seen in both occipital lobes and in several sulci of the parietal and frontal lobes. Light microscopic findings included loss of neocortical structure, with necrosis, neuronal loss, astrogliosis, vascular proliferation, mild spongiosis, and demyelination. The extent and severity of lesions were most pronounced in the occipital lobes and were greater in the left than in the right hemisphere. Other lesions included mild bilateral atrophy of the optic nerves, thymic involution, necrotizing dermatitis due to trauma, and a spectrum of spermatozoal abnormalities. The imaging and gross and light microscopic changes found in this animal resemble the mitochondrial encephalopathies of humans; this was corroborated by results of immunohistochemical analysis demonstrating decreased expression of enzymes of the mitochondrial oxidative complex ([OC]-I, -III, and -IV) in brain and muscle, and detection of fibrinogen immunoreactivity in neurons and glial cells. The spermatozoal defects may represent yet another aspect of a mitochondrial defect.

Disorders attributable to mitochondrial defects encompass a heterogeneous group of diseases, including encephalopathies and neuromuscular, gastrointestinal, cardiac, endocrine, reproductive, and renal disorders (19, 27, 32, 46, 52). Because of the dual genetic make-up of mitochondria, these diseases are typically caused by genetic errors in either mitochondrial DNA (mtDNA) or nuclear DNA (nDNA) and, due to the ubiquitous distribution of mitochondria, tend to be multisystemic. Tissues highly dependent on oxidative metabolism are especially vulnerable to defects in mitochondrial function, but the precise mechanisms leading to the different regional expression of neuropathologic lesions or combination of tissues affected in any one individual remain unresolved (19, 20, 44, 46, 47).

Although a variety of neurological diseases have been described in nonhuman primates, most are of an infectious nature (16). Paraventricular leucomalacia (PVL) has been described in fetal and infant monkeys (49, 50) but may be rare, judging by the few reports available. Likewise, lysosomal storage disorders are rare in nonhuman primates (2, 16), and mitochondrial encephalopathies have, to the best of our knowledge, never been described. Mitochondrial disorders have, however, been described in a number of other nonhuman species, including dogs (6-8), horses (53), and possibly cattle (1). We describe a case of subacute necrotizing encephalopathy accompanied by optic nerve atrophy, dysmorphisms, and spermatozoal defects in a young male pig-tailed macaque (*Macaca nemestrina*), with similarities to mitochondrial diseases in humans.

Received: 1/14/04. Revision requested: 2/26/04. Accepted: 3/17/04.
[1]Washington National Primate Research Center and [2]Department of Radiology, University of Washington, Seattle, Washington.
[*]Corresponding author: H. Bielefeldt-Ohmann, WaNPRC, University of Washington, Box 357330, Seattle, Washington 98195-7330.

Case Report

The young male macaque was received at the Washington National Primate Research Center (WaNPRC) as part of an import shipment from Indonesia (Indonesian Primate Center, Bogor), and was placed in international quarantine. The WaNPRC is an AAALAC-approved animal facility; all procedures performed are conducted in accordance with US Department of Agriculture (USDA) and Centers for Disease Control (CDC) requirements, the *Guide for the Care and Use of Laboratory Animals*, and are approved by the University of Washington Animal Care and Use Committee. During the requisite clinical examinations, blood- and tuberculosis (TB)-testing procedures, the animal was found to be in good nutritional and physical condition but unusually trusting and accommodating to human interaction, offering no resistance to handling. On several occasions, unusual "saluting" and hand-staring were observed by attending staff (Fig. 1).

The animal was referred to the Psychological Well-being Program (PWBP) staff for evaluation of abnormal behavior. By use of a dental examination, the animal was judged to be approximately 5 years old. Hematologic or blood biochemical abnormalities were not observed at any time; notably, lactic acidosis was not detected. During subsequent examinations and observations

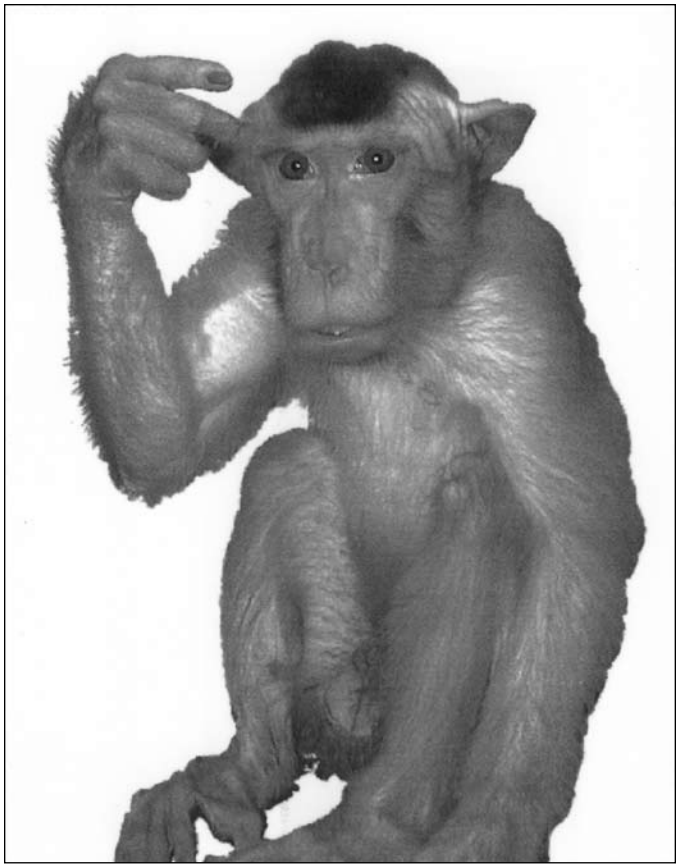

Figure 1. Photograph of the study subject demonstrating unusual "saluting."

by animal care staff, bilateral patellar luxation was detected. This was confirmed by radiography, which also indicated narrowing of the pelvis. In addition, the mandible was judged to be longer than normal for a pig-tailed macaque of the subject's estimated age. During follow-up examinations, horizontal nystagmus was apparent. On the basis of daily observations by animal care staff, a visual deficit was suspected, while hearing appeared adequate. Two and a half months after arrival, the animal was seen to display self-injurious behavior (SIB), and received medical treatment for the wounds and light sedatives (initially Buprenex [Reckitt Benckiser Pharmaceuticals Inc., Richmond, Va.], later followed by valium [Diazepam, IVAX Pharmaceuticals, Miami, Fla.]).

Over the next month, the animal became increasingly agitated, with repeated bouts of SIB despite continued medical treatment and enhanced environmental enrichment. During that period, magnetic resonance imaging (MRI) and positron emission tomography (PET) scanning were carried out. On the basis of the clinical deterioration and the imaging results, the animal was judged unfit for research assignment and euthanasia was performed.

Material and Methods

Behavioral observations. The subject's behavior was observed by the PWBP staff. Behavior was scored on a standard PWBP assessment data sheet used to quantify behavior profiles of animals referred to the PWBP for evaluation of possible behavior disorders. Normal and abnormal behaviors during a 10-min observation period were scored at 30-sec intervals (instantaneous scan samples [14]), using behavior categories identical to those of a previous study (3). In addition, any abnormal behavior was also scored on a 1/0 basis (i.e., scored as "1" during any interval when it occurred). The total scan samples in each behavior were converted to proportions (number of scan samples divided by total number of samples) and multiplied by 100 to estimate the percentage of time spent on each behavior. The behavior profile of the subject during eight samples (80 min) was compared with that of 87 4- to 11-year-old male pig-tailed macaques, including 29 previously referred to the PWBP for assessment of abnormal behavior and with that of 58 of a control group that were never referred for abnormal behavior (3). In addition, the subject was observed less formally during 24 assessments, and any abnormal behavior was recorded. These two methods provided a quantified time budget of abnormal versus normal behaviors, as well as an inventory of the various types of atypical behaviors displayed by the subject.

Magnetic resonance imaging. To assess regional abnormality in cerebral structures, MRI was performed. Prior to imaging, the animal was sedated by administration of ketamine, then was anesthetized with isofluorane. The MR images of the head were obtained using a 1.5-tesla GE Signa MR scanner (General Electric Medical Systems, Milwaukee, Wis.) equipped with a phased array coil. Three pulse sequences were used: a fast spine echo sequence (repetition time [TR] = 5,000 ms; echo time [TE] = 100 ms; number of excitations 2 [NEX]) to acquire 34 coronal images of an 80 × 80-mm field of view, 256 × 256 pixels, and 3-mm slice thickness (no gap); a fast spine echo inversion recovery sequence (TR = 5,000 ms; TE = 19 ms; inversion time [TI] = 350 ms; 2 NEX) to acquire 23 coronal images of 80-mm field of view, 256 × 256 pixels, and 3-mm slice thickness with 1.5-mm gap; and a spine echo sequence (TR = 550 ms; TE = 9 ms; 1 NEX) to acquire 26 sagittal images of 140 × 140-mm field of view, 256 × 128 pixels, and 3-mm slice thickness, with 1-mm gap.

Positron emission tomography imaging. To assess regional changes in cerebral energy metabolism, a radiotracer [18F]fluorodeoxyglucose ([F-18]FDG) was used for the imaging. Prior to radiotracer injection, the animal was sedated by administration of ketamine, then was anesthetized with isofluorane. A venous catheter was placed in the femoral vein for radiotracer administration. The animal's head was fixed in the PET scanner by use of a stereotactic frame. After intravenous injection of 3 milliCuries (mCi) of [F-18]FDG, a whole brain PET image set was obtained at 45 min after injection, using a dedicated primate scanner, SHR-7700 (Hamamatsu Photonics, K. K., Hamamatsu City, Japan). Thirty-one planes with 3.6-mm slice thickness were obtained simultaneously. Coronal images of the brain were reconstructed, using a filtered back-projection method, and were re-oriented in the stereotactic coordinates (15, 38) with corresponding MR images. The reconstructed spatial resolution is approximately 4 mm full-width-at-half-maximum (FWHM). Region of interest (ROI) analysis was performed to measure regional metabolic activity. The ROI were placed in the occipital cortex as well as the cerebellum.

Pathologic examination. Complete necropsy was performed immediately after euthanasia. Testes and epididimydes were placed aseptically into sterile saline-soaked swabs for spermatozoal collection. Other tissues were fixed in neutral-buffered 10% formaldehyde and were processed in routine manner for histopathologic study. After fixation for 48 h, the cerebrum was

serially cut in sagittal slices of 5-mm thickness. Selected samples from this series were processed for neuropathologic study. In addition to hematoxylin and eosin (H&E) stain applied to all tissues, sections from the cerebrum, cerebellum, and brainstem were also stained with Bielschowsky's silver stain (BSS) and luxol fast blue-periodic acid-Schiff (LFB-PAS) stain.

Immunohistochemical analysis. Deparaffinized sections were boiled in EDTA-buffer, pH 8.00, for 15 min to retrieve antigens, followed by immunolabeling with monoclonal antibodies specific for glial fibrillary acidic protein (GFAP; DAKO Corp., Carpinteria, Calif.), synaptophysin (Chemicon Intern Inc, Temecula, Calif.), as well as oxidative complex (OC-) I (30-kDa subunit), OC-II (30-kDa subunit), OC-III (iron-sulfur [FeS] subunit), and OC-IV (cytochrome c oxidase [COX] subunit I; all from Molecular Probes, Eugene, Oreg.), and polyclonal rabbit anti-fibrinogen antibody (DAKO Corp.). Bound antibodies were visualized by use of the streptavidin-biotin-peroxidase complex procedure, with diaminobenzidine or 3-amino-9-ethyl-carbazole as the chromogen (5, 51). Negative controls included omission of the primary antibody and use of irrelevant primary antibodies of the same isotype and species origin (in the case of mouse monoclonal antibodies: adenovirus or SV40 antibodies; in the case of rabbit antibody: SRV-2 antiserum [5]). Sections were counter-stained with Harry's hematoxylin, and were examined by use of a Nikon Eclipse E600 microscope.

The signal intensity for OC I–IV-immunolabeled tissues was assessed on a scale from 0 (no labeling apparent) to 4+ for highest intensity in normal control tissues obtained from two age-matched pig-tailed macaques. Similarly, fibrinogen labeling, as a measure of vascular leakage (33, 52), was assessed on a scale of 0 for lack of labeling in normal controls to 4+ for highest intensity in a vascular thrombus. Photomicrographs were obtained using a Nikon FDX-35 camera and Velvia RVP 135 film (Fujichrome, Tokyo, Japan) or a CoolPix 5400 digital camera (Nikon, Tokyo, Japan).

Spermatozoa isolation and examination. Spermatozoa were collected at room temperature by slicing the excised epididymides and allowing spermatozoa to swim out into HEPES-buffered human tubal fluid medium (mHTF, Irvine Scientific, Calif.) supplemented with bovine serum albumin (BSA; Sigma Chemical Co., St. Louis, Mo.; 3 mg/ml). Motile spermatozoa were washed in 10 ml of mHTF+BSA, then were centrifuged at 700 ×*g* for 10 min. The resulting spermatozoal pellet was re-suspended in fresh mHTF+BSA prior to analysis for concentration, morphology, motility, and acrosome status. Concentration was determined by use of a standard hemocytometer (58).

Morphology was assessed as the number of head, mid-piece, and tail defects per 100 cells (58). Motility was scored as the percentage of motile cells per 100 cells counted and as forward progressive motility on a scale from 1-5 (1 = immotile, 5 = rapid curvilinear motility). Acrosome status was scored by use of differential colorimetric analysis using a commercial stain according to the manufacturer's instructions (Spermac, Conception Technologies, San Diego, Calif.). The spermatozoal preparation was cryopreserved in Tris-EDTA-Saline (TES)-Tris egg yolk-based medium according to published methods (22, 45).

Results

Behavioral findings. The subject was observed to engage in an unusually large variety of abnormal behaviors (Table 1). Furthermore, vision impairment was suspected, as suggested by abnormal eye/head stimulation behaviors; apparent oblivion to food treats being presented, resulting in their falling into its pan or out of its grasp; and never appearing to look directly at the treat giver or the treat itself. On no occasion did PWBP staff observe any affiliative or agonistic interactions between the subject and other animals in the room. Furthermore, it did not engage in any eye contact or communicative facial gestures with its caregivers or PWBP observers, although indications were that its hearing faculties were intact.

Table 1. Abnormal behaviors displayed by study subject

Code	% of time*	Description
BP	23%	Bizarre posture: positioning hands and sometimes feet in front of face; staring at them; moving hands closer to, then farther from eyes repetitively as if there was a vision problem; once observed to direct a species-specific facial expression toward its hands (LEN or pucker).
LS	18%	Locomotor stereotypy: rapidly circling the cage repeatedly; sometimes reaching down to touch its cage toy while circling it; sometimes eating while pacing.
SAN	6%	Noninjurious self-biting of hands, feet; usually following LF or BP.
SH	3%	Head/eye stimulation: eye poking with hands or biscuits, directed toward both eyes. "Saluting" (Erwin & Deni, 1979 [21]).
SC	2%	Self-clasp: clasping limbs, usually holding legs with hands
SIB	Occ†	Self-injurious behavior.
LF	Occ	Floating limb: one foot (alternately left and right) would begin a slow upward movement (float) by its head, sometimes ignored but other times followed by SAN.

*% of time estimates from scan samples on behavior assessment datasheets (8

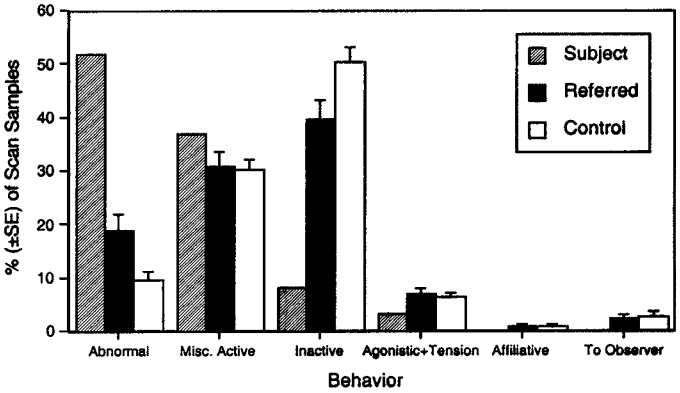

Figure 2. Behavior profile of the study subject, in comparison with mean (± SEM) values for 29 male pig-tailed macaques referred to the Psychological Well-being Program (PWBP) staff for behavioral assessment and 58 control (never referred) males (data from 3).

The study subject spent substantially more time engaged in abnormal behavior than did previously referred subjects, and spent less time being inactive (Fig. 2). The animal was scored for five abnormal behaviors on the systematic scan samples. During the 1/0 intervals and other observations, it was observed to engage in 3 more behaviors, for a total repertoire of 8 abnormal behaviors (Table 1). In comparison, the 29 referred male pig-tailed macaques from a previous study (3) displayed a mean 2.59 (± 1.02 [SD]) different abnormal behaviors during the scan sampling and 3.24 (± 1.18 SD) different abnormal behaviors overall.

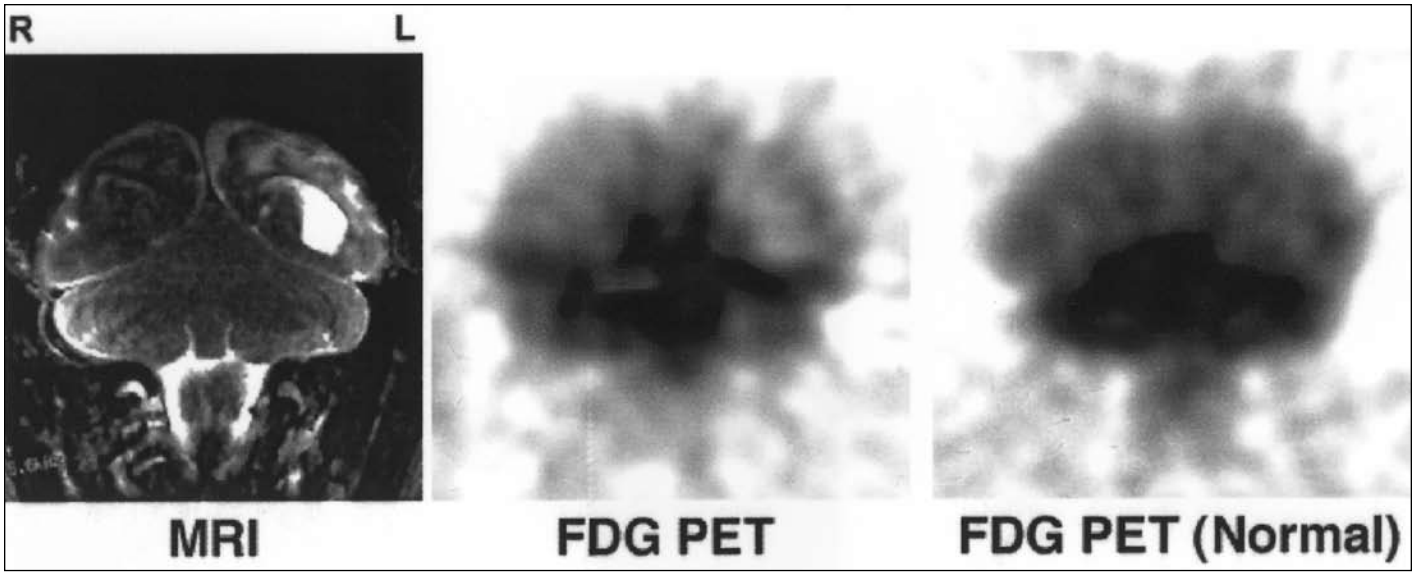

Figure 3. Magnetic resonance (MR) and positron emission tomography (PET) images of the brain. The left and middle images are from the subject. The right-hand image demonstrates representative metabolic activity of a normal, similarly aged monkey. The MR images (MRI, fast spine echo repetitions [TR] = 5,000 ms; echo time [0TE] = 100 ms) demonstrate encephalomalacia in the left occipital cortex, with ex-vacuo dilatation of the lateral ventricle. The [18F]fluorodeoxyglucose ([F-18]FDG) PET images (FDG PET) indicate more widespread metabolic reductions in both occipital cortices; the left is more severe than the right. Compared with the most-preserved metabolic activity in the midline cerebellum, the cerebellar hemisphere also shows decreased energy metabolism.

The subject, therefore, had a repertoire greater than 2 standard deviations above the mean for typical referred male *M. nemestrina* subjects. The subject's abnormal behavior also increased over time. During the first 4 scan sampling observations (prior to SIB), the subject averaged 41% of the time in abnormal behavior, and during the last 4 (post-SIB) observations, the average increased to 63% (Fig. 2 shows the mean for all 8 samples).

MR and PET imaging findings. The MR images indicated focal area of encephalomalacia in the left occipital cortex that was associated with ex-vacuo dilatation of the lateral ventricle (Fig. 3). The [F-18]FDG PET scan indicated more widespread metabolic abnormalities in the brain. The PET images indicated bilateral decreased metabolic activity in the occipital cortex, with the left side more severely affected than the right, corresponding to the MR abnormality (Fig. 3). Metabolic activity in the cerebellar hemisphere also appeared heterogeneous. The ratios of occipital metabolic activity to the most preserved activity in the cerebellum (near the vermis) in the normal, age-matched control were: right occipital = 0.58 and left occipital = 0.57. The corresponding results in the study subject were: right occipital = 0.48 and left occipital = 0.44, indicating approximately 17 (right) to 23% (left) metabolic reductions in the occipital cortex.

Gross pathologic changes. The animal was in adequate nutritional and hydration condition. The mandible appeared longer than normal, and substantial spacing was present between the molars and canines and between the latter and the incisors, most notable in the mandible. The skull, however, was of a shape and thickness that was within normal limits for the species and age group. The cerebral hemispheres appeared mildly to moderately swollen. The frontal lobes were short and round. Both occipital lobes were reduced in size, the left occipital by approximately 50%, with the neural tissue appearing gelatinous due to malacia (Fig. 4). The right occipital lobe appeared patchy chalk-white, devitalized, or necrotic (Fig. 4A). After formaldehyde fixation for 48 h and serial sectioning (at 4- to 6-mm intervals), marked dilatation of the left ventricle, and mild to moderate dilatation of the right ventricle, was revealed (Fig. 4C). The cortex of several lateral sulci was reduced in width, with yellowish discoloration (Fig. 4C and 4D).

Other lesions included multiple, variably sized (ranging from pin-point to 8-10 mm in diameter) superficial or deep erosions, covered by fresh or older scabs, in the skin on both sides of the face, and on the anterior and posterior aspects of the legs. All skin lesions were judged to be due to SIB, with their shape reflecting scratch marks inflicted by the nails. The patellae were bilaterally dislocated symmetrically over the lateral femoral condyles, with the patellar ligaments running over the head of the respective fibula and attaching to the tibial tuberosities. The patellae lacked the normal grooved shape for fitting the femoral condyles, and were instead evenly flat and smooth. The synovium of the right knee joint was mildly inflamed. The thymus was notably involuted, relative to that expected for an animal of this age group, and with a grayish color. The corpus cavernosum penis was fibrotic.

Histopathologic changes. The histologic changes observed in the cerebrum varied gradually in severity, with distribution corresponding to the grossly observed gradient (i.e., the most severe changes were seen in the left hemisphere, and they were more severe in the occipital lobes, with decreasing involvement of the temporal and frontal lobes). The left occipital lobe was characterized by complete loss of the normal neocortical laminar structure (compare Fig. 5A and 5B) with variable, but in many places complete, loss of neuronal cells; variable spongiosis; pronounced gliosis (mainly astrocytosis; Fig. 5C and 5E); apparent increase in capillaries (true neovascularization or due to collapse of the neuropil; Fig. 5B and 5D); and infiltration and accumulation of macrophages with foamy cytoplasm containing grayish cytoplasmic pigment, which was PAS-positive, in intra- and perivascular areas and in the ventricles (Fig. 5E and 5F).

The neuropil appeared to be collapsing (compare Fig. 5A and

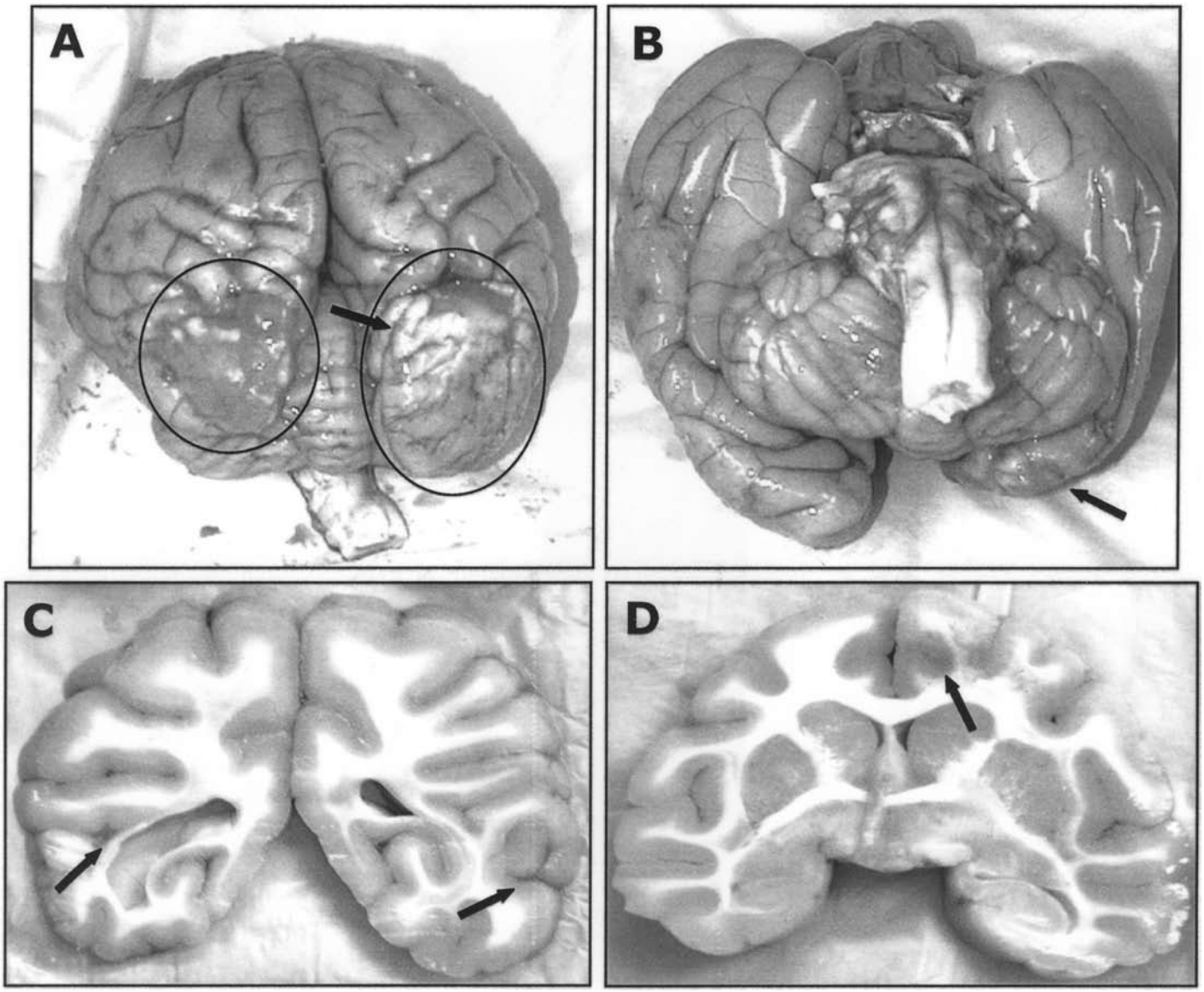

Figure 4. Severe leukomalacia affecting the occipital lobes (circled in A and B; arrow in B indicated the view of the severely reduced left occipital lobe) and sulci in the parietal and temporal lobes (arrows in C and D), accompanied by demyelination and megaventriculosis (C) in a 3-year-old pigtailed macaque with presumed mitochondrial defects. The chalk-white areas in the right occipital lobe (arrow in A) correspond to areas of necrosis and severe gliosis. Bar = 1 cm.

5B), and the meninges were thick due to increased arachnoid cell density and extracellular matrix, neovascularization, and infiltration of macrophages and a few lymphocytes. Luxol fast blue-PAS staining revealed loss of myelin (compare Fig. 5G and 5H with 5I). The right occipital lobe was characterized by similar, but less extensive or advanced, changes. Neurons were still apparent, albeit in decreased numbers, and many appeared degenerate, with condensed nuclei and cytoplasm and increased eosinophilia or basophilia. Myelin pallor was apparent in H&E-stained sections, a finding corroborated by LFB-PAS staining.

In the periventricular regions of the left and right hemispheres were mild to marked changes similar to those described for the occipital lobe. The changes were most pronounced in the areas surrounding the deep parts of the sulci, and the pyramidal cell layers appeared disproportionally affected. The left hippocampus was irregular; cells in the hippocampus proper were disorganized, and some appeared degenerate. This was accompanied by mild spongiosis and microgliosis. The dentate gyrus was likewise irregular in shape, but the neurons appeared light microscopically normal. In the left frontal lobe, there was focally moderate to marked gliosis accompanied by spongiosis in the cortex and apparent loss of neurons. In other areas, the neurons appeared with condensed nuclei and cytoplasm containing multiple clear vacuoles. The right frontal lobe was less affected, with mild-to-moderate gliosis, neuronal satellitosis, and neuronal degeneration seen in some areas.

Other light microscopic findings included mild atrophy of the optic nerve in both eyes, accompanied by an increase in interstitial collagen, increased numbers or density of oligodendroglial cells, and minimal to mild, diffuse lymphocyte infiltration. All other ocular structures appeared light microscopically normal.

The thymic involution, although advanced relative to that expected for the age group, appeared to follow the normal pattern for age-associated involution, with preservation of the corticome-

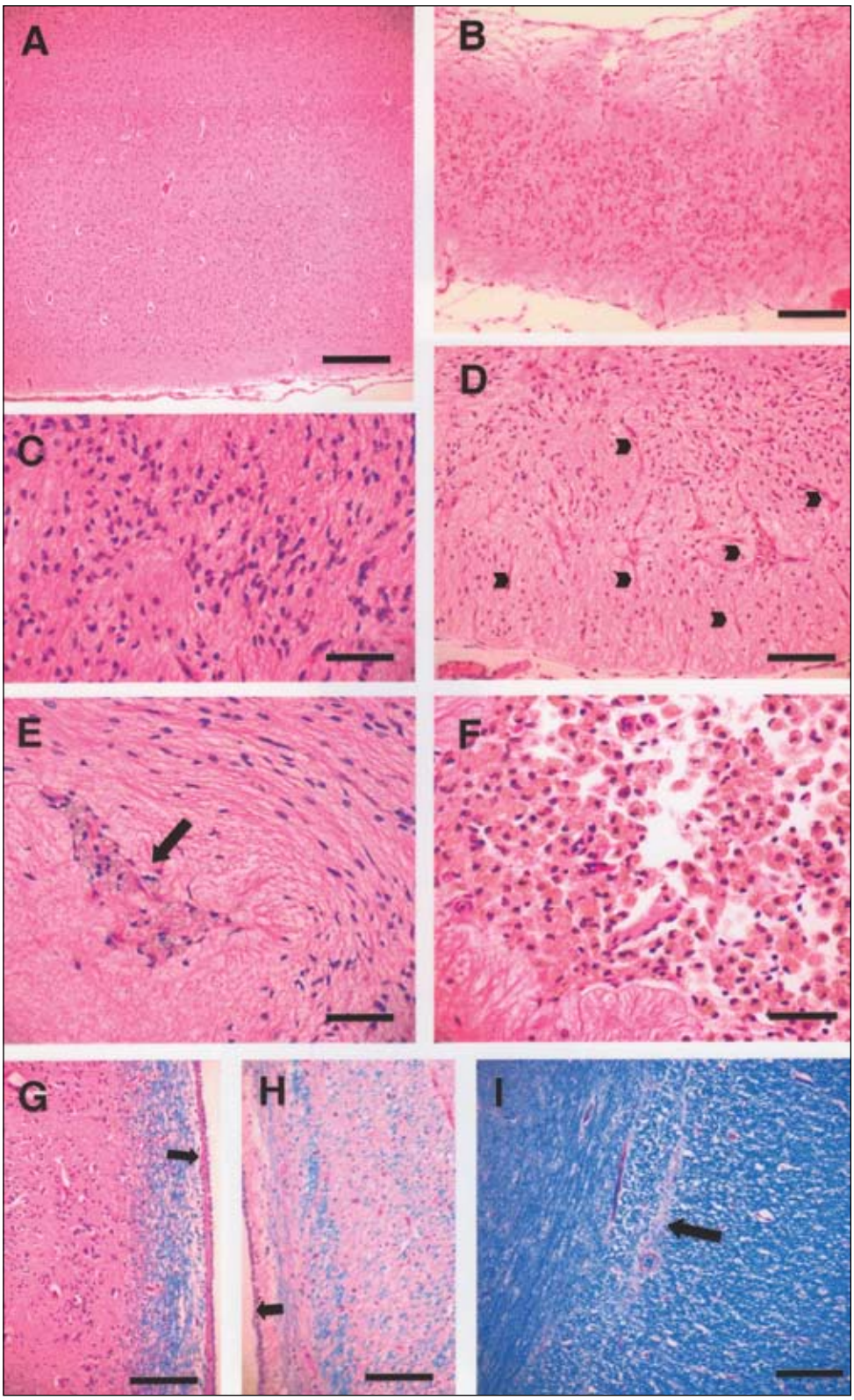

Figure 5. Photomicrographs of sections of the occipital lobes from the study subject (B-H) compared with an age-matched clinically normal *M. nemestrina* (A, I), demonstrating (B) loss of neocortical structure and tissue collapse; (C) atrogliosis; (D) increased vascularity (arrowheads) due to either true neovascularization or a relative increase due to neuropil collapse; (E) intravascular presence of macrophages with foamy cytoplasm (arrow) in the neuron-depleted, collapsed neuropil; (F) presence of foamy macrophages in dilated ventricles; and (G, H) demyelination, here in the periventricular neuropil of the dilated lateral ventricle. Arrows in G and H indicate ependymal cells lining the widely dilated ventricle in the study subject, and in (I) the narrow slit-like space in the normal brain. (A-F) H&E stain. (G-I) Luxol fast blue-periodic acid-Schiff stain. Bars: (A) 400 µm, (B) 200 µm, (C) 80 µm, (D) 100 µm, (E) 80 µm, (F) 80 µm, (G) 100 µm, (H) 100 µm, and (I) 100 µm.

Table 2. Functional and morphologic assessment of spermatozoa in samples obtained from normal colony males and the clinical subject

Variable	Colony males (range, n = 3)	Clinical subject
Concentration ($\times 10^6$/ml)	2,658 (1,400-4,525)	250
Motility (%)	90 (88-91)	55 (50-60)
Motility (forward progressive score)	5 (5-5)	3 (3-3)
Acrosome intact (%)	96.0 (91.5-99.5)	83.5 (82-85)

Table 3. Frequency of spermatozoal defects in samples obtained from normal colony males and the clinical subject

Defect	Colony males (range, n = 3)	Clinical subject
Head (%)	3.3 (1-5)	23 (20-26)
Mid-piece (%)	0.3 (0-1)	3.0 (2-4)
Tail (%)	0 (0-0)	3.0 (1-5)

Data are expressed as the percentage of defects observed in counts of 100 cells. Data for colony males are expressed as average values from n = 3 animals, with range in parentheses. Data for the clinical subject are expressed as an average of values obtained from two independent examinations, with range

dullary distinction and presence of Hassall's corpuscles. In addition, mild proliferative and lymphoplasmacytic gastritis was noted.

Examination of isolated spermatozoa indicated lower concentration, reduced percentage of motility, and reduced forward progressive motility score compared with spermatozoa collected from otherwise normal males, using the same procedures (Table 2). The clinical subject's spermatozoa sample also contained a lower percentage of acrosome-intact cells, with much higher percentages of partial and complete acrosome loss (Table 2). Compared with normal spermatozoa (Fig. 6A), stained spermatozoa from the clinical subject had tail defects consisting of doublets (Fig. 6B), short tails (Fig. 6E), and coils (Fig. 6F). Mid-piece defects included double mid-pieces in normal (Fig. 6C) and abnormal (Fig. 6D) positions. Head defects were most numerous, and included flat (Fig. 6E), elongated (Fig. 6G), or pin (Fig. 6H) heads. Tail, mid-piece, and head defects were seen with (Fig. 6B and 6H) or without (Fig. 6D and 6F) acrosome loss. The sample from the clinical subject had tail, mid-piece, and head defects at 7- to 10-fold higher values than did samples taken from clinically normal pig-tailed macaques (Table 3).

Immunohistochemical analytic findings. Immunolabeling for synaptophysin and GFAP corroborated the neuronal loss and

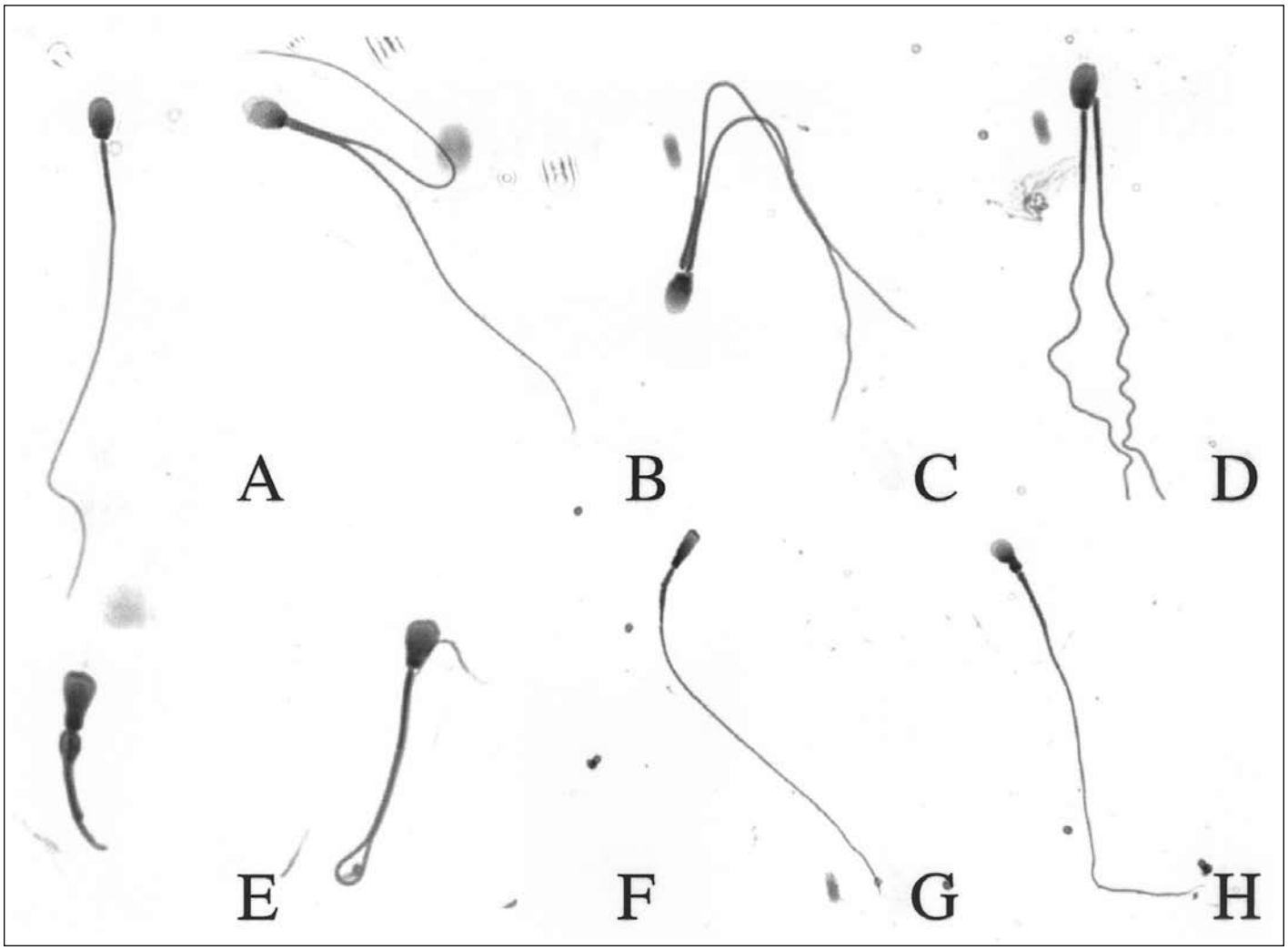

Figure 6. Photomicrographs of the spectrum of spermatozoa head and tail defects observed in the young pig-tailed macaque compared with normal controls. (A) Normal spermatozoa, (B) double tail, (C) double mid-piece, (D) double mid-piece (abnormal position) with convoluted tail(s), (E) flat head and short tail, (F) coiled tail, (G) elongated head, and (H) pin head.

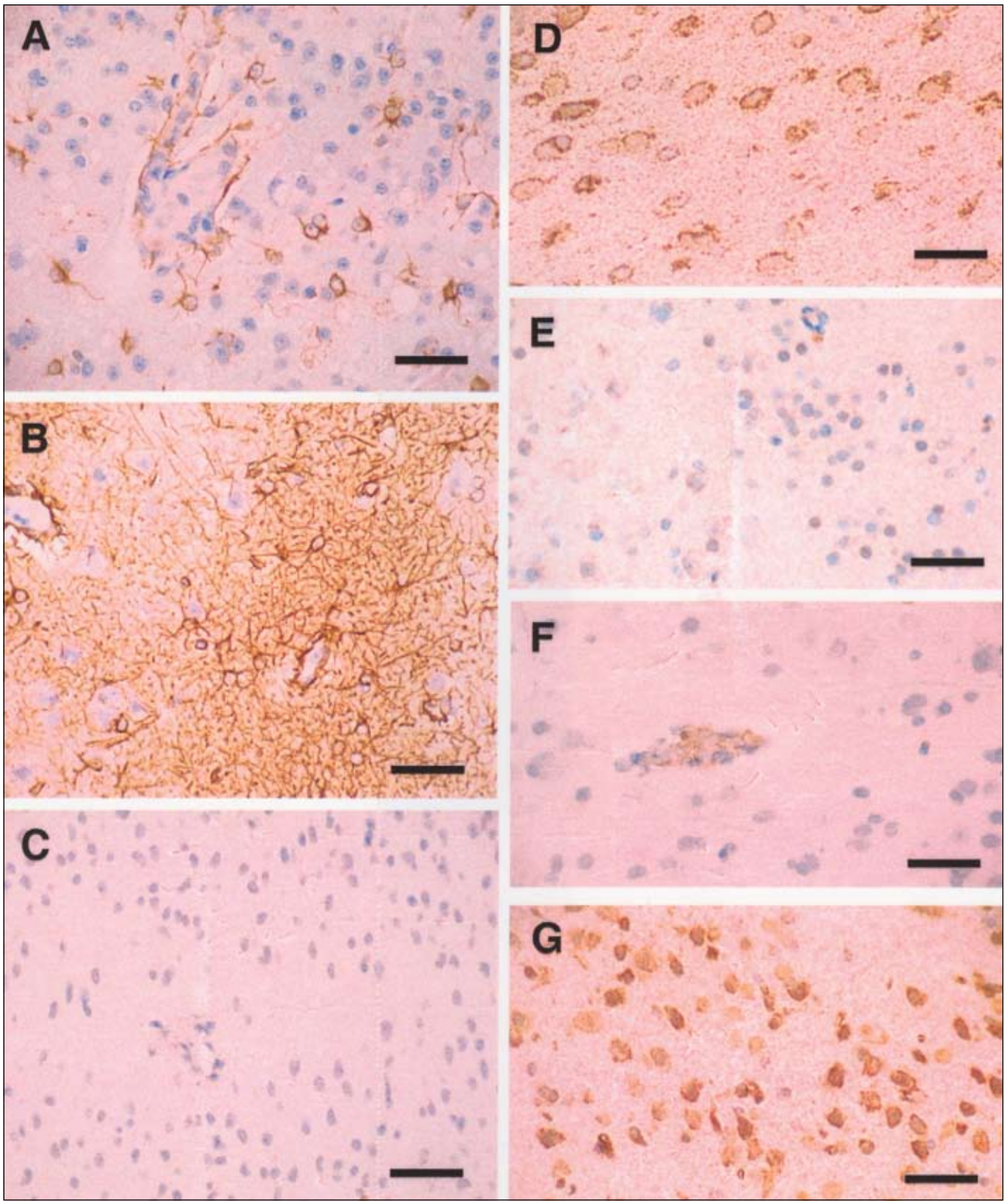

Figure 7. Comparison of astrocyte distribution and density, as revealed by immunohistochemical labeling for glial fibrillary acidic protein (GFAP), in the occipital neocortex of a normal *Macaca nemestrina* (A) compared with the study subject (B). (C) Negative control. Immunolabelling for oxidative complex (OC)-III (FeS) in the neocortex of a normal *M. nemestrina* (D) compared with the study subject (E). Localization of fibrinogen in the occipital lobe of a normal control macaque (F) and in the study subject (G). The diffuse immune reactivity for fibrinogen seen on neurons and glia cells is indicative of vascular leakage (33, 52). Bars: (A-C) 80 µm and (D-G) 60 µm.

Table 4. Summary of expression of mitochondrial oxidative complex (OC) subunits and fibrinogen, as assessed by immunohistochemical analysis, and semi-quantitative scoring

Antibody	Oxidative complex	Cell type	Normal control 1	Normal control 2	Study subject
A-21343	OC-I (30-kDa subunit)	Myocytes	4+	4+	4+
		Endothelia	4+	4+	3+
		Neurons	4+	4+	4+
		Astrocytes	4+	4+	3+
		Microglia	4+	4+	3+
A-21345	OC-II (30-kDa subunit)	Myocytes	4+	4+	4+
		Endothelia	4+	4+	4+
		Neurons	4+	4+	4+
		Astrocytes	4+	4+	4+
		Microglia	4+	4+	4+
A-21346	OC-III (FeS subunit)	Myocytes	4+	2-4+	4+
		Endothelia	4+	4+	2+
		Neurons	4+	4+	1-2+
		Astrocytes	4+	4+	1-2+
		Microglia	4+	4+	1-2+
A-6403	OC-IV (COX subunit 1)	Myocytes	4+	4+	4+
		Endothelia	4+	4+	3-4+
		Neurons	4+	4+	3+
		Astrocytes	4+	4+	3+
		Microglia	4+	4+	3+
Fibrinogen		Myocytes	ND	0	0
		Endothelia	ND	0	2+
		Neurons	ND	0	+
		Astrocytes	ND	0	+
		Microglia	ND	0	0

ND = not done.

gliosis, respectively, seen in H&E-stained sections (Fig. 7A and 7B, and data not shown). Using selected antibodies specific for the mitochondrial OC I–IV, decreased numbers of cells positive for OC-III and decreased expression in the remaining positive cells compared with cells in normal control brains, were seen in sections from most regions of the brain (Fig. 7D and 7E). Variable expression of this complex was also seen in myocardium and skeletal muscle (Table 4). In contrast, expression of OC-II in brain and muscle of the subject animal was comparable to that of two normal age-matched control macaques. Expression of OC-I and OC-IV appeared mildly decreased in neurons and glial cells, but in the musculature was comparable to that of control animals (Table 4). Astrocytes, neurons, and endothelial cells in the brain of the affected animal were immunoreactive for fibrinogen, whereas a reaction was only seen to intravascular material in normal macaques (Fig. 7F and 7G), suggesting vascular leakage into the neuropil of the study subject (33, 52).

Discussion

We have described a case of multi-organ defects in a young pigtailed macaque that encompass visual and neuropathologic defects as well as dysmorphic features and a wide range of severe spermatozoal defects. The signs of behavioral and neurologic dysfunction observed in this macaque most likely had an insidious onset followed by final rapid deterioration, since the animal had been deemed fit for research and export by veterinary clinicians at the place of origin. On its arrival at the WaNPRC, clinical signs of disease were comparatively mild, but grew progressively more pronounced over the ensuing three months. This, together with the neuropathologic findings, notably the multi-focal areas of neocortical collapse with neuronal loss, gliosis, increased vascularity and, to a lesser extent, spongiosis, and demyelination in periventricular regions, as well as the extracerebral lesions, including skeletal dysmorphic features, thymic atrophy and spermatozoal defects, argue against sequelae to meningitis (48) or encephalitis, hypoxic ischemia (9, 41), leukodystrophy (4), or periventricular leukomalacia (PVL) (28, 39, 43, 49) as the principal cause, and are more suggestive of an inherited or spontaneously arising mitochondrial defect(s) (20, 52). This contention is corroborated by the finding of decreased immunoreactivity for several mitochondrial enzymes, most notably FeS of the OC-III, an nDNA encoded enzyme. The type and distribution of cerebral lesions, notably the multifocal areas of neocortical structural loss, which did not correspond to any major vascular territories, and the predominant, bilateral cortical involvement, as well as the cortical blindness, bear some resemblance to the syndrome "mitochondrial encephalopathy, lactic acidosis, and stroke-like episodes" (MELAS) in humans (19, 20, 47, 52). However, this animal was notable for lack of biochemical abnormalities, measured in plasma, and clinical indications of stroke were never observed. Histomorphologic changes were not seen in the cerebellum, and the variably decreased metabolic activity in this region, as assessed by use of PET imaging, might have been due to cerebellar diaschisis rather than being a direct effect of the neurodegenerative process (25). Also, rather than displaying lethargy and dystonia, the monkey became increasingly more agitated and hyperactive, and manifested SIB in the last three to four weeks prior to euthanasia.

Serious abnormal behavior in nonhuman primates can have multiple causes, and is more common in colony-raised individuals receiving inadequate tactile social contact as infants or juveniles (3). Chronic stereotypies and non-injurious self-abuse may progress to SIB (37). Acute-onset SIB, however, may be a reaction to pain, and in humans, often appears to be inflicted in or near the area causing the pain sensation (13, 57). The possibility, therefore, remains that the acute-onset SIB seen in this young macaque was an indicator of pain. Notably, its target areas were the head and legs, possibly due to headaches and/or peripheral neuropathy.

Viable spermatogenesis occurs early in macaque species (starting between 2 years, 11 months and 4 years, 4 months), and is associated with testicular descent and growth and the adolescent spurt in linear growth (18, 54). The study subject's body weight and testicular morphology indicated that viable spermatogenesis would be operational. The metabolic demands of spermatozoa are high and are critically dependent on aerobic energy production via mitochondrial ATP catabolism. The clinical subject examined here exhibited many of the characteristics of the "Dag-like" effect reported for a number of other species with demonstrable derangements in mitochondrial numbers, distribution, and function (1, 17, 24). Although specific mitochondrial defects were not studied in spermatozoa samples from the subject, morphologic and functional data indicate that mitochondrial defects may have been present.

The precise pathogenesis of mitochondrial diseases, including the factors that lead to different regional expressions of neuropathologic and extraneural lesions, remain unresolved (20, 47, 52). Mitochondrial DNA encodes for ribosomal and transfer RNAs and polypeptides, which are subunits of the respiratory chain, located in the inner mitochondrial membrane, including subunits of OC-I (reduced nicotinamide adenine dinucleotide (NADH) dehydrogenase-ubiuionone oxidoreductase), OC-III (ubiquinone-cytochrome c oxidoreductase, OC-IV (cytochrome c

oxidase), and OC-V (ATP synthase). All of the OC-II (succinate dehydrogenase-ubiuionone oxidoreductase) subunits and the remaining subunits of OC-I, -III, and -V are encoded by nDNA (20, 52). Because in mammalian cells the mitochondrion consists of an interacting mobile network that contains thousands of copies of mtDNA, wild-type and mutant mtDNA can coexist, a phenomenon termed heteroplasmy (12). It has been proposed that clinical disease is a result of the "phenotypic threshold effect," which again is dependent on the overall metabolic requirements of any one tissue (10, 11, 44). Defects in any of the numerous mitochondrial pathways can cause mitochondrial diseases but, to date, those due to disorders of the respiratory chain are the best characterized (20). Pathogenic mutations in mtDNA and nDNA can affect respiratory chain activities by: decreasing the total amount of assembled active enzyme complexes, and/or decreasing the intrinsic kinetic parameters of these complexes (44).

The 4 "prototype" mitochondrial encephalopathies in humans are MELAS, Leigh's syndrome (LS), Kearns-Sayre syndrome, and myoclonus epilepsy with ragged-red fibers (MERRF), any of which can be associated with defects in several OC (20). In addition to some resemblance of this case to MELAS, the histomorphologic changes in our study subject also bear some resemblance to changes seen in patients with LS (47). However, there are major differences in topographic distribution, with basal ganglia, thalamus, midbrain, and pons typically affected in LS (47).

So far, no mitochondrial disease in humans has been associated with a defect in the nDNA encoding FeS. The decreased FeS immunoreactivity observed in this macaque may reflect: damage of FeS by oxygen-derived free radicals generated as a result of a defect within the respiratory chain (23, 42, 55); a decrease in assembled OC-III enzyme complex, with corresponding increased degradation of unbound FeS; or it may be a novel gene defect. Complex-III (ubiquinol-cytochrome c oxidoreductase) is responsible for taking reducing equivalents, which are generated in OC-I and -II and contained in ubiquinol, and transferring them through reactions with cytochrome b, the Rieske FeS protein, and cytochrome c_1 to the final electron acceptor cytochrome c. Inhibition of this reaction can result in markedly increased superoxide production (42). Oxygen-derived free radicals can further damage FeS, mtDNA, membranes, and other cellular constituents, leading to rapid cell ageing and death (23, 36, 42). A slightly less-pronounced decrease was also observed in OC-I and OC-IV immunoreactivity, whereas the OC-II complex expression appeared normal. The relative contribution of any of these putative enzyme deficiencies to the overall pathophysiologic and histopathologic changes in this animal remains unknown.

Only four enzymes out of a large total array of mitochondrial respiratory chain enzymes were tested (20, 44); therefore, it cannot be excluded that one or more enzymes not tested for also were deficient. Multiple partial defects in the oxidative phosphorylation and energy production pathways, whether primary or secondary, can additively contribute to reduced mitochondrial function, a phenomenon designated "synergistic heterozygosity" (56). Unambiguous detailing of putative defects in this macaque would require gene analysis, a currently unavailable approach. Furthermore, even in humans, less than 7% of clinically suspected cases of mitochondrial diseases are caused by a single gene defect in mtDNA or nDNA (34). Although there is clear association between specific mtDNA mutations with certain clinical phenotypes in humans, there also is significant overlap and atypical presentations (20, 40).

Other metabolic disorders with a basis in genetic defects, leading to neurodegenerative diseases early in life, include propionic acidemias, methyl malonic acidemias, branched chain axo-acid dehydrogenase complex deficiency ("maple syrup urine disease") and Friedreich's ataxia (FRDA) (26, 35). The former three are clinically indistinguishable, and in humans, usually present in the early neonatal period with progressive encephalopathy, resulting in coma with variable muscle tone and myoclonus (26). Friedreich's ataxia is caused by mutations in the gene coding for frataxin, a protein that regulates iron availability in mitochondria (31). Reduction in frataxin activity results in iron accumulation in the mitochondria and subsequent progressive oxidative damage in mtDNA and nDNA (31). Despite similarities in ultimate pathogenetic pathways between the prototypical mitochondrial respiratory chain diseases and FRDA (19, 20, 31), the latter principally affects the sensory neurons of the spinal cord and dorsal root ganglia (29), and the condition usually presents with ataxia and progresses to limb weakness. There may be mild generalized cerebral atrophy and abnormal cerebral glucose metabolism (30), but changes on the scale seen in our study subject do not occur in patients with FRDA.

Thus, although the diagnosis of mitochondrial encephalopathy in the macaque of this report remains tentative, the clinical, gross, and histopathologic and mitochondrial enzyme results collectively support this supposition. This would, therefore, be the first reported case of spontaneous mitochondrial disease in a nonhuman primate.

Acknowledgments

We thank Naoto Iwayama, Geoff Goebel, and the Animal Husbandry staff at WaNPRC for care of this animal, Mac Durning for assistance with immunohistochemical analysis, and Diella Koberstein and Kathy Bentson for assistance with behavioral observations and recordings. The WaNPRC is supported by core-funding from the National Institutes of Health NPRC (grant No. P51RR00166).

References

1. **Andersen Berg, K., O. Filseth, and E. Engeland.** 1996. A sperm midpiece defect in a Hereford bull with variable semen quality and freezability. Acta Vet. Scand. **37:**367-373.
2. **Baskin, G. B., M. Ratterree, B. B. Davison, K. P. Falkenstein, M. R. Clarke, J. D. England, M. T. Vanier, P. Luzi, M. A. Rafi, and D. A. Wenger.** 1998. Genetic galactocerebrosidase deficiency (globoid cell leukodystrophy, Krabbe disease) in rhesus monkeys (*Macaca mulatta*). Lab. Anim. Sci. **48:**476-482.
3. **Bellanca, R. U. and C. M. Crockett.** 2002. Factors predicting increased incidence of abnormal behavior in male pigtailed macaques. Am. J. Primatol. **58:**57-69.
4. **Berger, J., H. W. Moser, and S. Forss-Petter.** 2001. Leukodystrophies: recent developments in genetics, molecular biology, pathogenesis and treatment. Curr. Opin. Neurol. **14:**305-312.
5. **Bielefeldt-Ohmann, H., M. Gough, M. Durning, S. Kelley, H. D. Liggitt, and H-P. Kiem.** 2004. Greater sensitivity of pigtailed macaques (*Macaca nemestrina*) than baboons to total body radiation. J. Comp. Pathol., in press.
6. **Brenner, O., A. de Lahunta, J. F. Cummings, B. A. Summers, and M. Monachelli.** 1997. A canine encephalomyelopathy with morphological abnormalities in mitochondria. Acta Neuropathol. **94:**390-397.
7. **Brenner, O., A. de Lahunta A, B. A. Summers, J. F. Cummings, B. J. Cooper, B. A. Valentine, and J. S. Bell.** 1997. Hereditary polioencephalomyelopathy of the Australian cattle dog. Acta Neuropathol. **94:**54-66.
8. **Brenner, O., J. J. Wakshlag, B. A. Summers, and A. de La-**

hunta. 2000. Alaskan Husky encephalopathy—a canine neurodegenerative disorder resembling subacute necrotizing encephalomyelopathy (Leigh syndrome). Acta Neuropathol. **100:**50-62.
9. **Cai, Z., Y. Pang, F. Xiao, and P. G. Rhodes.** 2001. Chronic ischemia preferentially causes white matter injury in the neonatal rat brain. Brain Res. **898:**126-135.
10. **Cavanagh, J. B.** 1993. Selective vulnerability in acute energy deprivation syndromes. Neuropathol. Appl. Neurobiol. **19:**461-470.
11. **Cavanagh, J. B. and B. N. Harding.** 1994. Pathogenic factors underlaying the lesions in Leigh's disease. Tissue responses to cellular energy deprivation and their clinico-pathological consequences. Brain **117:**1357-1376.
12. **Chinnery, P. F., D. R. Thorburn, D. C. Samuels, S. L. White, H. M. Dahl, D. M. Turnbull, R. N. Lightowlers, and N. Howell.** 2000. The inheritance of mitochondrial DNA heteroplasmy: random drift, selection or both? Trends Genet. **16:**500-505.
13. **Craig, A. D.** 2003. A new view of pain as a homeostatic emotion. Trends Neurosci. **26:**303-307.
14. **Crockett, C. M.** 1996. Data collection in the zoo setting, emphasizing behavior, p. 545-565. *In* D. G. Kleiman, M. E. Allen, K. V. Thompson, S. Lumpkin, and H. Harris (ed.), Wild mammals in captivity: principles and techniques. University of Chicago Press, Chicago.
15. **Cross, D. J., S. Minoshima, S. Nishimura, A. Noda, H. Tsukada, and D. E. Kuhl.** 2000. Three-dimensional stereotactic surface projection analysis of macaque brain PET: development and initial application. J. Nucl. Med. **41:**1879-1887.
16. **Cusick, P. K. and S. J. Morgan.** 1998. Nervous system. p. 461-483. *In* B. Taylor Bennett, C. R. Abee, and R. Henrickson (ed.), Nonhuman primates in biomedical research—diseases. Academic Press, San Diego, Calif.
17. **Czaker, R. and B. Mayr.** 1984. Multiple malformations of bovine spermatozoa with special reference to their light microscopic fluorescing pattern and electron-microscopic structure. Andrologia **16:**61-71.
18. **Dang, D. C. and N. Meusy-Dessolle.** 1984. Quantitative study of testis histology and plasma androgens at onset of spermatogenesis in the prepuberal laboratory-born macaque (*Macaca fascicularis*). Arch. Androl. **12:**43-51.
19. **DiMauro, S., E. Bonilla, M. Davidson, M. Hirano, and E. A. Schon.** 1998. Mitochondria in neuromuscular disorders. Biochem. Biophys. Acta. **1366:**199-210.
20. **DiMauro, S. and E. A. Schon.** 2003. Mitochondrial respiratory-chain diseases. N. Engl. J. Med. **348:**2656-2668.
21. **Erwin, J. and R. Deni.** 1979. Strangers in a strange land: abnormal behaviors or abnormal environments, p. 1-28. *In* J. Erwin, T. L. Maple, and G. Mitchell (ed.), Captivity and behavior: primates in breeding colonies, laboratories and zoos. Van Nostrand Reinhold, New York.
22. **Feradis, A. H., D. Pawitri, I. K. Suatha, M. R. Amin, T. L. Yusuf, D. Sajuthi, I. N. Budiarsa, and E. S. Hayes.** 2001. Cryopreservation of epididymal spermatozoa collected by needle biopsy from cynomolgus monkeys (*Macaca fascicularis*). J. Med. Primatol. **30:**100-106.
23. **Flint, D. H., J. F. Tuminello, and M. H. Emptage.** 1993. The inactivation of Fe-S cluster containing hydro-lyases by superoxide. J. Biol. Chem. **268:**22369-22376.
24. **Folgero, T., K. Bertheussen, S. Lindal, T. Torbergsen, and P. Oian.** 1993. Mitochondrial disease and reduced sperm motility. Hum. Reprod. **8:**1863-1868.
25. **Gold, L. and M. Lauritzen.** 2002. Neuronal deactivation explains decreased cerebellar blood flow in response to focal cerebral ischemia or suppressed neocortical function. Proc. Natl. Acad. Sci. USA **99:**7699-7704.
26. **Harding, B. N. and R. Surtees.** 2002. Metabolic and neurodegenerative diseases of childhood, p. 485-517. *In* D. I. Graham, and P. I. Lantos (ed.), Greenfield's neuropathology, 7th ed., vol. I. Arnold, London.
27. **Imai, H., K. Suzuki, K. Ishizaka, S. Ichinose, H. Oshima, I. Okayasu, K. Emoto, M. Umeda, and Y. Nakagawa.** 2001. Failure of the expression of phospholipid hydroperoxidase glutathione peroxidase in the spermatozoa of human infertile males. Biol. Reprod. **64:**674-683.
28. **Inder, T. E., P. S. Huppi, S. Warfield, R. Kikinis, G. P. Zientara, P. D. Barnes, F. Jolesz, and J. J. Volpe.** 1999. Periventricular white matter injury in the premature infant is followed by reduced cerebral cortical gray matter volume at term. Ann. Neurol. **46:**755-760.
29. **Jitpimolmard, S., J. Small, R. H. King, J. Geddes, P. Misra, J. McLaughlin, J. R. Muddle, M. Cole, A. E. Harding, and P. K. Thomas.** 1993. The sensory neuropathy of Friedreich's ataxia: an autopsy study of a case with prolonged survival. Acta Neuropathol. (Berl). **86:**29-35.
30. **Junck, L., S. Gilman, S. S. Gebarski, R. A. Koeppe, K. J. Klun, and D. S. Markel.** 1994. Structural and functional brain imaging in Friedreich's ataxia. Arch. Neurol. **51:**349-355.
31. **Karthikeyan, G., J. H. Santos, M. A. Graziewicz, W. C. Copeland, G. Isaya, B. Van Houten, and M. A. Resnick.** 2003. Reduction in frataxin causes progressive accumulation of mitochondrial damage. Hum. Mol. Genet. **12:**3331-3342.
32. **Kuroiwa, T., T. Kuwata, T. Nakayama, T. Takemura, M. Sakuta, S. Ichinose, Y. Goto, and R. Okeda.** 1998. Mitochondrial encephalomyopathy showing prominent microvacuolation and necrosis of intestinal smooth muscle cells: a case diagnosed by rectal biopsy. Acta Neuropathol. **96:**86-90.
33. **Kwon, E. E. and J. W. Prineas.** 1994. Blood-brain barrier abnormalities in longstanding multiple sclerosis. An immunohistochemical study. J. Neuropathol. Exp. Neurol. **53:**625-636.
34. **Liang, M-H. and L-J. C. Wong.** 1998. Yield of mtDNA analysis in 2,000 patients. Am. J. Med. Genet. **77:**395-400.
35. **Lowe, J. S. and N. Leigh.** 2002. Disorders of movement and system degeneration, p. 325-429. *In* D. I. Graham, and P. I. Lantos (ed.), Greenfield's neuropathology, 7th ed., vol. 2. Arnold, London.
36. **Luo, X., S. Pitkanen, S. Kassovska-Bratinova, B. H. Robinson, and D. C. Lehotay.** 1997. Excessive formation of hydroxyl radicals and aldehydic lipid peroxidation products in cultured skin fibroblasts from patients with complex I deficiency. J. Clin. Invest. **99:**2877-2882.
37. **Lutz, C. K., A. Well, and M. A. Novak.** 2003. Stereotypic and self-injurious behavior in rhesus macaques. A survey and retrospective analysis of environment and early experience. Am. J. Primatol. **60:**1-15.
38. **Martin, R. F. and D. M. Bowden.** 1996. A stereotaxic template atlas of the macaque brain for digital imaging and quantitative neuroanatomy. Neuroimage **4:**119-150.
39. **Marumo, G., S. Kozuma, J. Ohyu, Y. Hamai, Y. Machida, K. Kobayashi, E. Ryo, N. Unno, T. Fujii, K. Baba, T. Okai, S. Takashima, and Y. Taketani.** 2001. Generation of periventricular leukomalacia by repeated umbilical cord occlusion in near-term fetal sheep and its possible pathogenetical mechanisms. Biol. Neonate **79:**39-45.
40. **Moraes, C. T., D. P. Atencio, J. Oca-Cossio, and F. Diaz**. 2003. Techniques and pitfalls in the detection of pathogenic mitochondrial DNA mutations. J. Mol. Diagn. **5:**197-208.
41. **Ohyu, J., G. Marumo, H. Ozawa, S. Takashima, K. Nakajima, S. Kohsaka, Y. Hamai, Y. Machida, K. Kobayashi, E. Ryo, K. Baba, S. Kozuma, T. Okai, and Y. Taketani.** 1999. Early axonal and glial pathology in fetal sheep brains with leukomalacia induced by repeated umbilical cord occlusion. Brain Dev. **21:**248-252.
42. **Raha, S. and B. H. Robinson.** 2000. Mitochondria, oxygen-free radicals, disease and ageing. Trends Biochem. Sci. **25:**502-508.
43. **Rezale, P. and A. Dean.** 2002. Periventricular leukomalacia, inflammation and white matter lesions within the developing nervous system. Neuropathology **22:**106-132.
44. **Rossignol, R., B. Faustin, C. Rocher, M. Malgat, J-P. Mazat, and T. Letellier.** 2003. Mitochondrial threshold effects. Biochem. J. **370:**751-762.
45. **Sankai, T., K. Terao, R. Yanagimachi, F. Cho, and Y. Yoshikawa.** 1994. Cryopreservation of spermatozoa from cynomolgus monkeys (*Macaca fascicularis*). J. Reprod. Fertil. **101:**273-278.
46. **Smeitink, J., L. Van den Heuvel, and S. DiMauro.** 2001. The genetics and pathology of oxidative phosphorylation. Nat. Rev. Genet. **2:**342-352.
47. **Sparaco, M., E. Bonilla, S. DiMauro, and J. M. Powers.** 1993. Neuropathology of mitochondrial encephalopathies due to mitochondrial DNA defects. J. Neuropathol. Exp. Neurol. **52:**1-10.

48. **Stevens, J. P., M. Eames, A. Kent, S. Halket, D. Holt D, and D. Harvey.** 2003. Long term outcome of neonatal meningitis. Arch. Dis. Child Fetal Neonatal Ed. **88:**F179-F184.
49. **Sumi, S. M.** 1979. Sudanophilic lipid accumulation in astrocytes in periventricular leukoencephalomalacia in monkeys. Acta Neuropathol. **47:**241-243.
50. **Sumi, S. M., R. W. Leech, E. C. Alford, M. Eng, and K. Ureland.** 1973. Sudanophilic lipids in the unmyelinated primate cerebral white matter after intrauterine hypoxia and acidosis. Res. Publ. Assoc. Res. Nerv. Ment. Dis. **51:**176-197.
51. **Swasdipan, S., M. McGowan, N. Phillips, and H. Bielefeldt-Ohmann.** 2002. Pathogenesis of transplacental virus infection: pestivirus replication in the placenta and fetus following respiratory infection. Microb. Pathog. **32:**49-60.
52. **Tanji, K., T. Kunimatsu, T. H. Vu, and E. Bonilla.** 2001. Neuropathological features of mitochondrial disorders. Semin. Cell Dev. Biol. **12:**429-439.
53. **Valberg, S. J., G. P. Carlson, G. H. Cardinett, E. K. Birks, J. H. Jones, A. Chomyn, and S. DiMauro.** 1994. Skeletal muscle mitochondrial myopathy as a cause of exercise intolerance in a horse. Muscle Nerve **17:**305-312.
54. **van Wagenen, G. and M. E. Simpson.** 1954. Testicular development in the rhesus monkey. Anat. Rec. **118:**231-251.
55. **Vladutiu, G. D.** 1997. Advances in the genetic mechanisms of mitochondrial disease. Curr. Opin. Neurol. **10:**512-518.
56. **Vockley, J., P. Rinaldo, M. J. Bennett, D. Matern, and G. D. Vladutiu.** 2000. Synergistic heterozygosity: disease resulting from multiple partial defects in one or more metabolic pathways. Mol. Genet. Metab. **71:**10-18.
57. **Watkins, L. R. and S. F. Maier.** 2002. Beyond neurons: evidence that immune and glial cells contribute to pathological pain states. Physiol. Rev. **82:**961-1011.
58. **World Health Organization.** 1999. Laboratory manual for the examination of human semen and semen-cervical mucus interaction, 4th ed. Cambridge University Press, Cambridge, England.